# Vortex structure of elegant Laguerre–Gaussian beams of fractional order

**Israel Martinez-Castellanos and Julio C. Gutiérrez-Vega***

*Photonics and Mathematical Optics Group, Tecnológico de Monterrey, Monterrey 64849, Mexico*
**Corresponding author: juliocesar@itesm.mx*

Received August 12, 2013; revised October 5, 2013; accepted October 8, 2013;
posted October 9, 2013 (Doc. ID 195558); published October 28, 2013

The transition of the vortex structure of fractional elegant Laguerre–Gaussian beams is discussed in detail as the angular mode index of the beam is continuously varied between integer values. Under this kind of variation, the vortices can be classified into five groups. Contrary to the behavior of the vortices of the nondiffracting Bessel beams of fractional order, the nodal lines of the vortices in the case of the fractional eLG beams exhibit intricate shapes. 

*OCIS codes:* (050.1940) Diffraction; (260.1960) Diffraction theory; (350.5500) Propagation.
http://dx.doi.org/10.1364/JOSAA.30.002395

## 1. INTRODUCTION

Optical phase singularities have recently become a popular topic in optical physics and beam shaping through their relationship with beams carrying orbital angular momentum (OAM) [1,2]. It is now well-known that the OAM per photon carried by these beams can take an arbitrary value within a continuous range, either integer or noninteger in units of $\hbar$ [3–11]. This class of beams can be produced, for example, using either a spiral phase plate whose phase jump is not an integer multiple of $2\pi$ [3,4], suitable superpositions of Laguerre–Gaussian beams [5,6], or Bessel beams [7–9].

Recently, the elegant Laguerre–Gaussian (eLG) beams of fractional order have been introduced as closed-form solutions of the paraxial wave equation [5]. These mode solutions represent continuous transition modes between the known eLG with integer mode indices. The possibility of adjusting the radial and angular mode indices within a continuous range of values allows one to control the physical properties of the beam (e.g., OAM, $M^2$ factor, intensity moments, etc.), providing additional degrees of freedom. In the study of optical beams with noninteger OAM, an accurate mapping of their intricate phase distribution is a critical tool for successfully tracing the dynamics of the fields and observing the mutual interactions of multiple vortices as they propagate [4,8,12].

In this paper, we characterize the vortex structure of the fractional eLG beams. We put special emphasis on the creation, annihilation, folding, unfolding, and transverse displacement of the phase singularities as the angular mode index increases continuously between integer values. We found that under this variation the vortices can be classified in five groups. Contrary to the behavior of the vortices of the nondiffracting Bessel beams of fractional order [7,8], the three-dimensional trajectories of the vortex nodal lines in the case of the diffracting eLG beams exhibit much more intricate shapes. We have also observed that the vortex structure of the beams is significantly affected by variations of the angular index rather than variations of the radial index, so we focus our attention in the characterization of this particular variation.

## 2. ELEGANT LAGUERRE–GAUSSIAN BEAMS OF FRACTIONAL ORDER

We briefly describe fractional eLG beams in order to establish notation and to provide a reference point for necessary formulas [5]. We begin the analysis by writing the complex field amplitude of the normalized Gaussian beam with time dependence $\exp(-i\omega t)$ propagating in free-space along the positive $z$ axis of a coordinate system $\mathbf{r} = (x, y, z) = (r\cos\theta, r\sin\theta, z)$

$$U_{0,0}(\mathbf{r}) = \sqrt{\frac{2}{\pi}}\frac{1}{\mu w_0}\exp\left(-\frac{r^2}{\mu w_0^2}\right), \qquad \mu \equiv \mu(z) = 1 + i\frac{z}{z_R}, \tag{1}$$

where $w_0$ is the beam width at the waist plane $z = 0$, $z_R = kw_0^2/2$ is the Rayleigh distance, and $k$ is the wave number.

The eLG beam of fractional radial $\eta$ and angular $\lambda$ mode numbers can be obtained from the Gaussian beam $U_{0,0}(\mathbf{r})$ by the fractional application of the rising and lowering operators

$$A^{\pm} \equiv \mp\frac{w_0}{\sqrt{2}}\left(\frac{\partial}{\partial x} \pm i\frac{\partial}{\partial y}\right) = \mp\frac{w_0}{\sqrt{2}}\exp(\pm i\theta)\left(\frac{\partial}{\partial r} \pm i\frac{1}{r}\frac{\partial}{\partial\theta}\right), \tag{2}$$

according to the following operator prescription:

$$U_{\eta,\lambda}(\mathbf{r}) = c_{\eta,\lambda}(A^{+})^{\eta+\lambda}(A^{-})^{\eta}U_{0,0}, \tag{3}$$

where $\eta \geq 0$ and $\lambda \in \mathbb{R}$ are two arbitrary numbers denoting the fractional radial and angular indices of the beam, and $c_{\eta,\lambda} = 1/\sqrt{\Gamma(2\eta + |\lambda| + 1)}$ is a normalization constant.

The explicit evaluation of Eq. (3) gives the fractional beam with arbitrary fractional indices $(\eta, \lambda)$ as a superposition of

 

fractional beams with integer angular indices $\lambda = l = (\ldots, -2, -1, 0, 1, 2, \ldots)$:

$$U_{\eta,\lambda}(\mathbf{r}) = (-i)^{\lambda} \sum_{l=-\infty}^{\infty} (-1)^{l} \operatorname{sinc}(l-\lambda) U_{\eta,l}(\mathbf{r}), \tag{4}$$

where $\operatorname{sinc}(w) = \sin(\pi w)/\pi w$ is the sinc function, and $U_{\eta,l}(\mathbf{r})$ is the rotationally symmetric fractional eLG beam with angular dependence $\exp(il\theta)$ (i.e., integer OAM states), namely

$$U_{\eta,l}(\mathbf{r}) = \frac{i^{2\eta+|l|}\Gamma(\eta'+|l|+1)}{\Gamma(|l|+1)} \left(\frac{2}{\sqrt{\mu}w_0}\right)^{2\eta'+|l|} R^{|l|} U_{0,0}(\mathbf{r}) \times {}_1F_1(-\eta', |l|+1; R^2) \exp(il\theta), \tag{5}$$

with $\Gamma(\cdot)$ being the Gamma function, ${}_1F_1(\cdot)$ the confluent hypergeometric function, and

$$R \equiv \frac{r}{\sqrt{\mu}w_0}, \qquad \eta' \equiv \eta + \frac{\lambda - |l|}{2}. \tag{6}$$

Figure 1 shows the transverse amplitude and phase distributions of the fractional beam $U_{\eta,\lambda}(\mathbf{r})$ at the plane $z = 0$ for the radial indices $\eta = \{1, 2\}$ and the angular indices $\lambda = \{2, 2.25, 2.5, 2.75, 3\}$. The patterns were obtained by adding 101 terms of the series in Eq. (4) in the interval $\lambda - 51 \le l \le \lambda + 50$. As the orders $\eta$ and $\lambda$ vary, the irradiance and phase patterns vary continuously, exhibiting an azimuthally asymmetric shape. If the angular order is integer ($\lambda = l$), then only one term of the series (4) survives and the entire field reduces to the single expression in Eq. (5). In this case, the beam $U_{\eta,l}(r, \theta, z = 0)$ is axially symmetric and has $n$ radial zeros when $\eta$ falls in the interval $(n-1) < \eta \le n$. Each of these radial zeros correspond to a circular phase dislocation in the transverse plane $z = 0$. The intensity pattern of the fractional eLG beams is symmetrical about the $y$ axis and its OAM density grows continuously as the angular index increases, see [5] for details. We finally remark that the fractional eLG beams can be experimentally produced following the same standard techniques used to generate paraxial beams with liquid crystal displays or holographic plates.

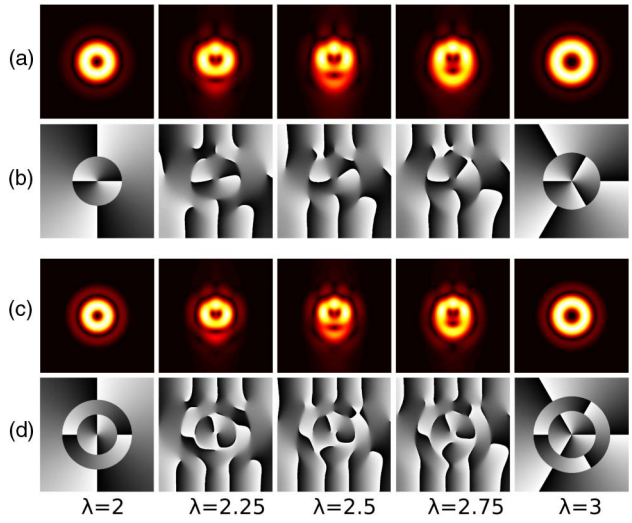


Fig. 1. Transverse amplitude and phase distributions of the fractional beam $U_{\eta,\lambda}(\mathbf{r})$ at the plane $z = 0$ for the angular indices $\lambda = \{2, 2.25, 2.5, 2.75, 3\}$ and the radial indices (a), (b) $\eta = 1$; (c), (d) $\eta = 2$. Transverse dimensions $\pm 4w_0$.

## 3. VORTEX STRUCTURE FOR FRACTIONAL ANGULAR MODE NUMBERS

We study the behavior of the vortex structure of the fractional eLG beams as its angular mode number $\lambda$ is continuously varied. A first insight is gained by considering the simplest case when the radial index $\eta$ equals zero. Figure 2 shows the phase maps of the eLG beams $U_{0,\lambda}(x, y, 0)$ for different values of the angular index $\lambda$. For fractional $\lambda$, the phase maps are characterized by a number of unit-strength vortices located symmetrically about the $y$ axis. Positive and negative vortices are represented by white and black dots, respectively, and can be located by finding the intersection of the zero contour lines $\operatorname{Re} U = 0$ and $\operatorname{Im} U = 0$. The position of the vortices changes as $\lambda$ increases such that for integer values of $\lambda = l$ some of them collapse at the origin generating a $l$-strength axial vortex and the rest go away to infinity or annihilate at the circular rings of phase dislocation.

Figure 2 also shows with green dots the saddle points of the phase distribution. These points have been located by finding the intersections of the zero contour lines $\nabla(\arg U) \cdot \hat{\mathbf{x}} = 0$ and $\nabla(\arg U) \cdot \hat{\mathbf{y}} = 0$.

Let us now assume that the radial index $\eta$ equals 1. Choosing $\eta = 1$ ensures that there is only one circle of phase dislocation for integer values of $\lambda$. This assumption does not restrict the generality of the following results because the case $\eta = 1$ contains all the relevant aspects of the vortex dynamics when the angular order $\lambda$ is not integer.

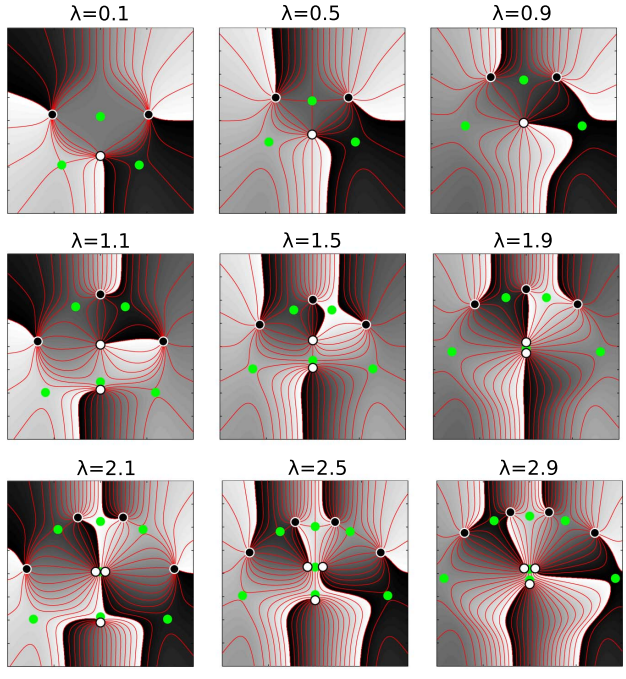


Fig. 2. Phase map for beams with $\eta = 0$ in $0.1 \le \lambda \le 2.9$ at plane $z = 0$. Red lines are equally spaced contour phase lines. Black and white dots are vortices with topological negative and positive charge, respectively; green dots are saddle points. Transverse dimensions $\pm 4w_0$.

When $\lambda = l$ is an integer, the field $U_{\eta=1,l}(\mathbf{r})$ becomes a single axially symmetric eLG beam with integer indices whose phase is characterized by (a) an isotropic higher-order vortex of strength $l$ located at the origin and (b) a phase dislocation circle corresponding to the zero of the Laguerre polynomial (see Fig. 1). In contrast, when the angular order $\lambda$ is not an integer, the field $U_{\eta=1,\lambda}(\mathbf{r})$ presents a rich structure of vortices embedded in the morphology of its transverse field distribution. The creation, annihilation, and migration of vortices as $\lambda$ increases is depicted in Fig. 3 for the full range $\lambda \in [0,3]$. For clarity, we show separately the vortex behavior for the partial intervals $\lambda = [0,1],[1,2],[2,3]$ in subplots (a), (b), and (c), respectively. The position of the vortices was determined numerically by finding the crossing points of the zero contour lines of the real and imaginary parts of the field $U_{\eta,l}(\mathbf{r})$ at the transverse plane $z = 0$. The dotted circles correspond to the circular phase dislocation corresponding to integer values of $\lambda$.

From Fig. 3, we note that under variations of the angular index the vortices can be classified in five groups, all of them distributed symmetrically about the $y$ axis. In what follows the symbol $\lfloor x \rfloor$ means the nearest integer less than or equal to $x$ (i.e., the *floor* function), and $\lceil x \rceil$ means the nearest integer greater than or equal to $x$ (i.e., the *ceil* function). As illustrated in Fig. 3, the vortex groups are

1. $\eta + \lfloor \lambda \rfloor + 2$ negative unit-strength vortices in the top that originate from and return to infinity as $\lambda$ increases from $\lfloor \lambda \rfloor = l$ to $\lceil \lambda \rceil = l + 1$.
2. $2(\rho + \lfloor \lambda \rfloor) + 1$ vortices alternating charge sign that migrate from the $\rho$-th dislocated ring when $\lfloor \lambda \rfloor = l$ to the $\rho$-th ring when $\lceil \lambda \rceil = l + 1$.
3. $\rho$ positive vortices that go from the $\rho$th ring of $\lfloor \lambda \rfloor$ to the $(\rho - 1)$th ring of $\lceil \lambda \rceil$. Note that in this statement we considered the origin as the zeroth ring and infinity as the $(\eta + 1)$th ring.
4. $\rho$ pairs of vortices with opposite charges that come from between the $\rho$th and the $(\rho + 1)$th rings of $\lceil \lambda \rceil$. The negative ones go to the $\rho$th ring while the positive to the $(\rho + 1)$th ring. The positive one will become negative and will annihilate with a positive vortex coming from the next ring.
5. $\lfloor \lambda \rfloor$ single positive vortices that unfold from the vortex of charge $\lfloor \lambda \rfloor$ at the origin.

While for lower orders, specially close to the integers, the vortex groups are easy to track, for higher orders the vortices begin to interact with members of others or the same group through processes of annihilation-creation, and the above classification may be not so clear. Anyway, the classification of vortices in groups will be useful in the following discussions.

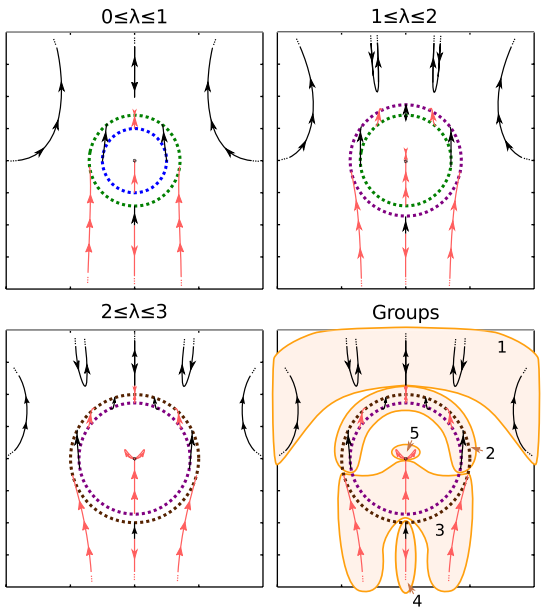


Fig. 3. Migration of vortices of the beam $U_{1,\lambda}(x,y,0)$ as the angular order increases from 0 to 3. Red and black lines represent positive and negative vortices, respectively. Dotted circles are the rings of phase dislocation when $\lambda$ becomes integer. Lines with dotted ends indicate that vortices come from or go to infinity. Transverse dimensions $\pm 4w_0$.

### A. Unfolding and Refolding of Vortices at the Optical Axis

The trajectories of the vortices within the central region of $U_{\eta=1,\lambda}(\mathbf{r})$ as the angular order $\lambda$ continuously increases from 2 to 5 are depicted in Fig. 4. For arbitrary values of $\lambda$, the phase

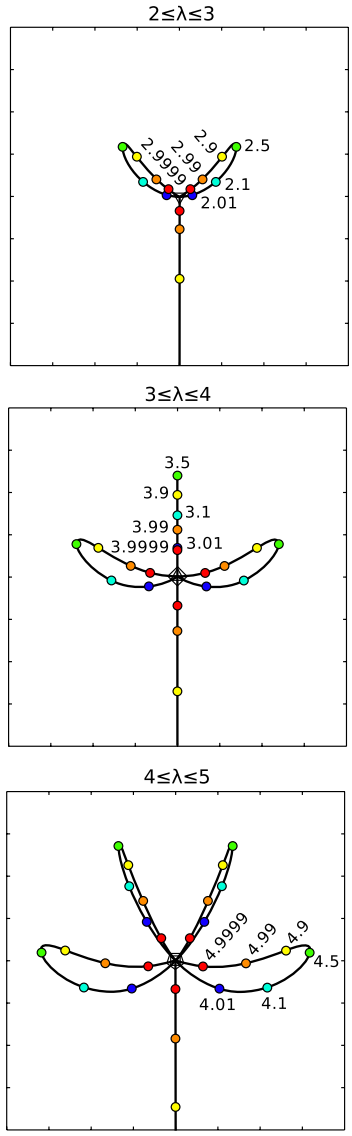


Fig. 4. Unfolding and refolding of higher-order axial vortices during the transition between consecutive integer angular mode numbers. Numbers represent the order $\lambda$. Transverse dimensions $\pm 0.8w_0$.

distribution of the fractional beam deviates significantly from the integer case. In general, the positions of the vortices on the transverse plane cannot be calculated in closed form, but they can be determined as intersection points of nodal lines representing the curves $\mathrm{Re}\,U = 0$ and $\mathrm{Im}\,U = 0$.

For small perturbations, we note that (a) the on-axis higher order vortex unfolds into $\lfloor\lambda\rfloor$ unit-strength vortices lying at the vertices of a $\lfloor\lambda\rfloor$-sided regular polygon centered on the optical axis and (b) a new vortex emerges at the intersection of the negative $y$ axis and the first circular zero contour of the Laguerre polynomial. As $\lambda$ increases, the $\lfloor\lambda\rfloor$ unfolded vortices move away from the origin until reaching the maximum separation when $\lambda \sim \lfloor\lambda\rfloor + 1/2$ while the new vortex moves further along the negative $y$ axis toward the origin. As $\lambda \to \lceil\lambda\rceil$, the original $\lfloor\lambda\rfloor$ unfolded vortices and the new vortex tend to the origin, forming a new $\lceil\lambda\rceil$-sided regular polygon centered on the optical axis. Finally, when $\lambda = l + 1$, all the vortices collapse on axis generating the new integer order phase singularity.

The excursion of the axial vortices in Fig. 4 is very similar to the trajectories of the fractional Bessel beams discussed in [8]. An important difference with respect to the Bessel case is that while for fractional Bessel modes the outgoing and incoming transit speeds as $\lambda$ increases are approximately the same, in the case of the eLG, the axial higher-order vortex is much more unstable when $\lambda$ decreases than when it is increased respect the integer value.

### B. Behavior of the Vortices along the $y$ Axis

The $y$ axis represents the plane of symmetry of the intensity pattern of the fractional beams, so it is instructive to study the movement of vortices along this special line as the fractional order increases. Figure 5 shows the position of the vortices located on the $y$ axis as a function of the angular index $\lambda \in [0, 6]$ for the beams with radial indices $\eta = 0, 1$, and 2. Red and black lines represent positive and negative helicity of the vortices, respectively.

Let us begin with the fundamental nonvortex Gaussian beam $\eta = \lambda = 0$. If the angular index $\lambda$ is slightly increased then a positive vortex appears at a very large negative value of the $y$ axis and travels into the positive $y$ direction as $\lambda$ increases. When $\lambda = 1$, the vortex reaches the origin and represents the single positive vortex of the axially symmetric $\mathrm{eLG}_{01}$ beam. If now $\lambda$ is slightly increased beyond the unity (i.e., $\lambda = 1 + \delta\lambda$), then two new singularities birth on the $y$ axis: a negative vortex (group 1) coming from $+\infty$ and a positive vortex (group 3) coming from $-\infty$. As $\lambda$ goes from 1 to 2, we distinguish three phenomena: (i) the original axial vortex makes an excursion in the positive $y$ axis returning to the origin when $\lambda = 2$; this is a group 5 vortex, (ii) the new positive vortex travels positively from $-\infty$ and finally collapses at the origin with the original vortex when $\lambda = 2$; this is the second-order axial vortex of the axially symmetric $\mathrm{eLG}_{02}$ beam, and (iii) the new negative vortex moves approaching to the origin but at $\lambda \approx 1.4$ returns to infinity.

When the radial order increases, i.e., $\eta = 1$ or $\eta = 2$, vortices of the group 2 appear and correspond to the singularities originated at the circular dislocation rings. Note in subplot 5(b) that the distinction between these vortices and the ones from the group 1 becomes less clear, specially when both groups interact in an annihilation process at $\lambda \approx 2.38$. For

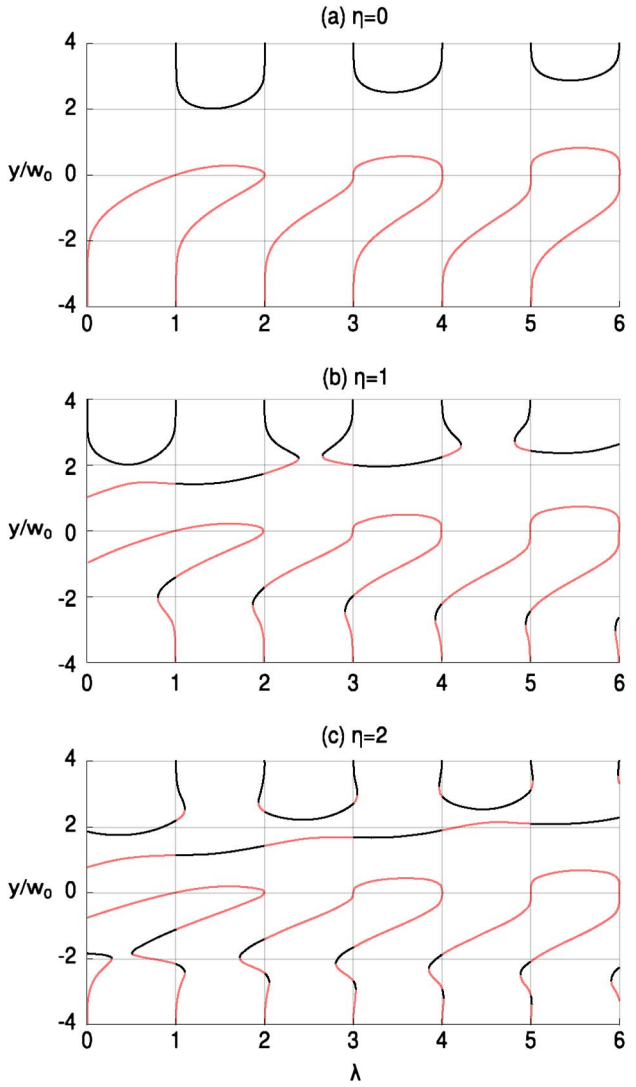


Fig. 5. Vertical displacement of the vortices along the $y$ axis as the angular order increases for the beams with radial indices $\eta = 0, 1$, and 2. Red and black lines represent positive and negative helicity of the vortices, respectively.

all radial orders, vortices of the group 5 are the positive lines just above $y = 0$. It is easy to see how they break apart and collapse at integer values of $\lambda$, where they join one of the vortices of the group 3 (i.e., the positive lines just below $y = 0$) providing the mechanism for increasing of charge of the high-order vortex at the origin. Finally, the successive change between negative and positive lines in the lower part correspond to the group 4, in which pair of vortices create and annihilate rapidly. As can be seen, these groups in the lower part also begin to interact with each other, and while tracking them is harder, in the $y$ axis is not so much.

Lines change sign because of two reasons: the first case is the annihilation or creation processes that occurs when a curve is tangent to a vertical line of constant $\lambda$, except in the origin, where a higher-order vortex is created instead. The second case occurs at integers values of $\lambda$, where it can be seen how the smallest angle between the contour lines $\mathrm{Re}\,U = 0$ and $\mathrm{Im}\,U = 0$ decreases until the ring is formed and then the angle begin to increase but in the other direction.

### C. Vortex Structure on Propagation

The eLG beams differ from the standard LG beams in that the former contain Laguerre polynomials with a complex argument, whereas in the latter the argument is real. As a consequence, whereas the standard beams are shape invariant on propagation (up to a scaling factor), the transverse pattern of the elegant solutions does not remain constant. This fact holds also for eLG beams with fractional order. Therefore, it is clear that the vortex distribution of the fractional eLG beams at the waist plane $z = 0$ will change substantially on propagation.

The transverse displacement of the vortices as the beam propagates is illustrated in Fig. 6 for eLG beam with radial index $\eta = 1$ and $\lambda = 1.3$ and 1.5 within the range $0 \le z/z_R \le 1$. In general for nonzero $\lambda$, the vortices will rotate on propagation around the optical axis getting away from the origin describing diverging spirals as $z$ increases. This behavior occurs because of the diffraction of the spherical Gaussian envelope of the eLG beams and the coexistence of OAM density about the origin within the structure of the eLG beam. Figure 6 also illustrates the sign principle: vortices adjacent on a zero contour of Re $U$ or Im $U$ have opposite sign. If a contour is closed, there must be an even number of phase singularities, alternating in sign, and the overall topological charge on that contour is zero, giving an overall topological neutrality condition: topological charge cannot accumulate on a closed contour loop.

The vortices of diffracting optical fields in three-dimensional space form nodal lines of null-intensity with intricate shapes [2,12]. In Fig. 7, we show the evolution of the nodal lines of the fractional eLG beam with indices $\eta = 1$ and $\lambda = 1.5$ that corresponds to the phase maps in the second row of Fig. 6. The lines have been mapped in the waist region of the beam delimited by $|z| \le z_R$ and $r < 2.25w_0$. The green oscillating nodal line clearly shows the processes of creation and annihilation of unitary vortices as the beam propagates near the plane $z = 0$. The blue nodal lines represent the trajectories of two positive independent unitary vortices near the optical axis. Figure 7 shows the fact that the topological charge of the beam is a conserved quantity under smooth changes of the optical field. The only way that a phase singularity can appear on propagation is together with other phase singularities such the sum of all topological charges is zero. Likewise, the only way that a vortex can disappear is for it to annihilate with other vortex of opposite sign.

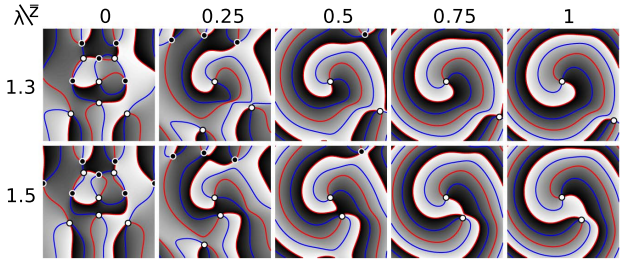


Fig. 6. Behavior of the phase map of the fractional beam $U_{1,\lambda}(\mathbf{r})$ for $\lambda = 1.3$ and 1.5 within the range $0 \le z/z_R \le 1$. Red and blue lines correspond to zero contour lines Re $U = 0$ and Im $U = 0$, respectively. White and black dots represent positive and negative vortices. Transverse dimensions $\pm 3w_0$.

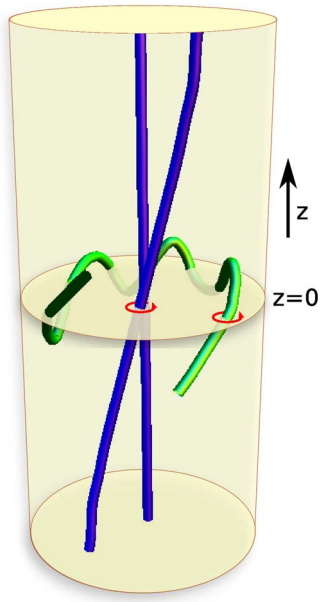


Fig. 7. Evolution of vortex nodal lines of the eLG beam with indices $\eta = 1$ and $\lambda = 1.5$ in the waist region $|z| \le z_R$. Red arrows show the helicity of the vortex lines at the plane $z = 0$.

## 4. CONCLUSION

In summary, we have studied the phase map and vortex structure of eLG beams with fractional order. We characterized the creation, annihilation, and movement of the vortices across the transverse plane as the angular mode number is continuously varied for fixed values of the radial mode number. It was found that the vortices can be classified into five groups according to the behavior of its transverse displacement. We have also shown that in free space propagation, the optical vortices rotate around the beam axis. This rotation is attributed to the fact that the eLG beams are not shape invariant and that the beam OAM density can be separated in its "vortex" and "asymmetry" parts, as shown by Bekshaev *et al.* [13].

## ACKNOWLEDGMENTS

This research was partially supported by CONACyT grant 182005 and by the Tecnológico de Monterrey Research Chair in Optics grant CAT141.

## REFERENCES

1. M. S. Soskin and M. V. Vasnetsov, "Singular optics," Prog. Opt. **42**, 219–276 (2001).
2. M. R. Dennis, K. O'Holleran, and M. J. Padgett, "Singular optics: optical vortices and polarization singularities," Prog. Opt. **53**, 293–363 (2009).
3. M. V. Berry, "Optical vortices evolving from helicoidal integer and fractional phase steps," J. Opt. A **6**, 259–268 (2004).
4. J. Leach, E. Yao, and M. J. Padgett, "Observation of the vortex structure of a non-integer vortex beam," New J. Phys. **6**, 71 (2004).
5. J. C. Gutiérrez-Vega, "Fractionalization of optical beams: II. Elegant Laguerre–Gaussian modes," Opt. Express **15**, 6300–6313 (2007).
6. J. B. Götte, K. O'Holleran, D. Preece, F. Flossmann, S. Franke-Arnold, S. M. Barnett, and M. J. Padgett, "Light beams with

fractional orbital angular momentum and their vortex structure," Opt. Express **16**, 993–1006 (2008).
7. J. C. Gutiérrez-Vega and C. López-Mariscal, "Nondiffracting vortex beams with continuous orbital angular momentum order dependence," J. Opt. A **10**, 015009 (2008).
8. C. López-Mariscal, D. Burnham, D. Rudd, D. McGloin, and J. C. Gutiérrez-Vega, "Phase dynamics of continuous topological upconversion in vortex beams," Opt. Express **16**, 11411–11422 (2008).
9. S. Orlov, K. Regelskis, V. Smilgevičius, and A. Stabinis, "Propagation of Bessel beams carrying optical vortices," Opt. Commun. **209**, 155–165 (2002).
10. I. V. Basistiy, V. A. Pas'ko, V. V. Slyusar, M. S. Soskin, and M. V. Vasnetsov, "Synthesis and analysis of optical vortices with fractional topological charges," J. Opt. A **6**, S166 (2004).
11. T. Fadeyeva, C. Alexeyev, A. Rubass, and A. Volyar, "Vector erf-Gaussian beams: fractional optical vortices and asymmetric TE and TM modes," Opt. Lett. **37**, 1397–1399 (2012).
12. J. Leach, M. R. Dennis, J. Courtial, and M. J. Padgett, "Vortex knots in light," New J. Phys. **7**, 55 (2005).
13. A. Ya. Bekshaev, M. S. Soskin, and M. V. Vasnetsov, "Optical vortex symmetry breakdown and decomposition of the orbital angular momentum of light beams," J. Opt. Soc. Am. A **20**, 1635–1643 (2003).